frontiers | Frontiers in Batteries and Electrochemistry

TYPE Original Research
PUBLISHED 07 August 2025
DOI 10.3389/fbael.2025.1647877

OPEN ACCESS

EDITED BY
Rachid Essehli,
Oak Ridge National Laboratory (DOE),
United States

REVIEWED BY
Guosheng Li,
Pacific Northwest National Laboratory (DOE),
United States
Selva Chandrasekaran Selvaraj,
University of Illinois Chicago, United States

*CORRESPONDENCE
Jung Ho Kim,
jhkim@uow.edu
Junyoung Mun,
munjy@skku.edu

†These authors have contributed equally to this work

RECEIVED 16 June 2025
ACCEPTED 18 July 2025
PUBLISHED 07 August 2025

CITATION
Lee K, Jiang F, Jeong S, Lee H, Kim JH and Mun J (2025) Effects of dry and wet coating methods on surface degradation of Ni-rich cathodes in Li-ion rechargeable batteries. *Front. Batter. Electrochem.* 4:1647877. doi: 10.3389/fbael.2025.1647877

Effects of dry and wet coating methods on surface degradation of Ni-rich cathodes in Li-ion rechargeable batteries

Keonwoo Lee[1†], Feng Jiang[2†], Seonghun Jeong[1], Hyojoo Lee[1,3], Jung Ho Kim[3*] and Junyoung Mun[1,2,3,4*]

[1]School of Advanced Materials Science and Engineering, Sungkyunkwan University, Suwon, Republic of Korea, [2]Department of Future Energy Engineering, Sungkyunkwan University, Suwon, Republic of Korea, [3]Institute for Superconducting and Electronic Materials (ISEM), Faculty of Engineering and Information Sciences, University of Wollongong, Wollongong, NSW, Australia, [4]SKKU Institute of Energy Science and Technology (SIEST), Sungkyunkwan University, Suwon, Republic of Korea

Ni-rich cathode materials have attracted significant attention as high energy density cathodes for lithium-ion batteries. However, Ni-rich cathode materials with a Ni content exceeding 80% have encountered challenges such as electrolyte side reactions due to the instability of Ni ions. These issues lead to rapid capacity fading and undermine battery stability. To address these problems, surface coating techniques have been widely employed. Among these methods, wet coating techniques have been commonly used. However, this approach leads to the unintended formation of a NiO-like phase due to water exposure, which accelerates cation mixing and degrades electrochemical performance. In this study, a dry coating method that excludes the influence of water was employed to enhance the surface stability of Ni-rich cathode materials. This enhanced stability is attributed to the suppression of NiO-like phase formation on the surface of the dry coated cathodes, which prevents cation mixing during cycling, avoids capacity degradation, and prolongs battery cycle life. Experimental results demonstrated significant differences between dry coated and wet coated Ni-rich samples based on $LiNi_{0.8}Co_{0.1}Mn_{0.1}O_2$ (NCM811). The capacity retentions of dry coated and wet coated NCM811 at 0.5C at 150 cycles were 80.8% and 73.4%, respectively. This result demonstrates that dry coating offers a statistically significant improvement in long-term capacity retention, reflecting a 10% enhancement in stability compared to conventional methods. Rate capability was evaluated by cycling at incremental rates from 0.2C to 20C (3 cycles per rate) followed by an additional 150 cycles at 0.5C. The results demonstrated that the dry coated sample exhibited a more pronounced and stable rate capability across all tested conditions compared to the wet coated sample. These findings confirm that the absence of NiO-like phase formation contributed significantly to enhancing the electrochemical performance, particularly in terms of stability and long-term reliability.

KEYWORDS

dry coating, wet coating, Ni-rich layered oxide, cathode, NiO-like phase

1 Introduction

With the rapid expansion of the electric vehicle (EV) market, the demand for batteries with high energy density and excellent stability is growing rapidly (Li M. et al., 2018; Roy et al., 2024). Among these, rechargeable lithium-ion batteries (LIBs) are garnering significant attention and extensive research. In particular, cathode materials, which play the most critical role in battery performance, are the focus of intense investigation (Nitta et al., 2015; Liu et al., 2016). Recent years have seen advancements in the development of diverse cathode materials tailored to meet specific demands. Layered structure cathodes, such as $LiNi_xCo_yMn_{1-x-y}O_2$ (NCM), and $LiNi_xCo_yAl_{1-x-y}O_2$ (NCA), are common in the research topics due to their high energy density and capacity (Hong et al., 2024; Mitra and Sudakar, 2024; Sim et al., 2024). As the demand for batteries with both higher energy density and improved safety rises, particular attention is being paid to the development of Ni-rich cathode materials with nickel content exceeding 80% (Sim et al., 2024; Ho et al., 2025a). Due to their high capacity and cost efficiency, Ni-rich cathodes are emerging as promising candidates for high energy density batteries (Sun et al., 2021; Ho et al., 2025b). Nonetheless, unlike traditional cathodes such as $LiCoO_2$ (LCO) and $LiNi_{1/3}Co_{1/3}Mn_{1/3}O_2$ (NCM333), Ni-rich cathodes suffer from significant surface instability due to the high reactivity of Ni^{3+} (Mun et al., 2014; Kasnatscheew et al., 2017). During cycling, these materials experience degradation, leading to cation mixing, where Li^+ and Ni^{2+} exchange positions (Cui et al., 2021). This issue occurs because of the similar ionic radii of Li^+ (0.76 Å) and Ni^{2+} (0.69 Å), and magnetic frustration (Wang W. et al., 2024). Severe cation mixing compromises structural stability, resulting in critical challenges such as reduced battery cycle ability, electrolyte decomposition, and interface instability (Cui et al., 2021; Wang W. et al., 2024).

To address these challenges, researchers are employing strategies such as elemental doping and coating (Sun et al., 2021; Qu et al., 2022). Doping is one of the most effective methods for suppressing the cation mixing failure. Metallic dopants stabilize the structure during synthesis, improving cycle performance (Sun et al., 2021). The choice of dopant and its concentration significantly influence performance, as excessive doping adversely affects both capacity and cycle ability. Recent advancements include strategies like dual doping or high entropy doping with multiple elements to enhance performance (Park et al., 2022; Ma et al., 2025). Coating creates a physical barrier that prevents direct contact between the electrolyte and the cathode materials (Qu et al., 2022). This approach suppresses side reactions with the electrolyte, mitigating the formation of a thick solid electrolyte interphase (SEI) layer and reducing electrolyte consumption, which are common causes of capacity fading (Yan et al., 2022). However, overly thick coating layers negatively affect ionic and charge transfer, ultimately reducing performance. Coating methods are generally categorized into wet and dry techniques. The conventional wet coating process for Ni-rich cathode materials, despite using excellent coating materials, can lead to performance degradation due to the reduction of Ni^{3+} to Ni^{2+} when exposed to wet solvents during the process (Kalluri et al., 2017). In addition, exposure to moisture causes H^+ from H_2O to exchange with Li^+ in the layered structure, leading to Li^+ loss during synthesis (Hartmann et al., 2021), which in turn results in the formation of electrochemically inactive phases (e.g., NiO-like phase) (Kasnatscheew et al., 2017; Hong et al., 2022; Jeong et al., 2022). These inactive phases exacerbate structural instability and creating fundamental issues that severely impact cycle life and safety (Wang F. et al., 2024). Thus, the surface passivation has not been independently investigated by unavoidable possible surface failure.

Dry coating with shear stress avoids the use of solvents, minimizing issues arising from wet coating processes (Ho et al., 2025a). In addition, it is environmentally friendly as it does not require the use of solvents, eliminating the need for additional drying. Furthermore, it offers the advantages of forming a durable and robust coating layer while enabling the production of a uniform coating layer (Herzog et al., 2021). Dry coating methods have merit with reduction of costs and environmental pollution by eliminating the need for solvents utilized in wet processes, offering a promising advantage.

In this study, we evaluate the effects of both dry coating and water-based (D.I. water) wet coating methods on the performance of Ni-rich cathode materials. The dry coating method utilizes high energy generated from blade rotation to coat Al_2O_3 particles onto the active material through collision. Al_2O_3 is selected for its advantages and economic efficiency as a coating material (Han et al., 2017).

2 Experimental

2.1 Dry coating method

The dry coating process was performed using a spheric coater (KMtech, Korea). This process began with a pre-mixing step, where NCM811 cathode material (Umi-core) and the coating material $Al(NO_3)_3{\cdot}9H_2O$ (Sigma Aldrich) were mixed using mortar and pestle for 5 min to aid initial dispersion. In this step, $Al(NO_3)_3{\cdot}9H_2O$ was added in an amount equivalent to an appropriate Al_2O_3 coating ratios. Subsequently, the mixture of active material and coating material was placed into the spheric coater, and dry coating was conducted at a blade rotation speed of 3,000 rpm for 20 min. After the dry coating, the sample was calcined in a box furnace at 700°C for 6 h under an O_2 atmosphere. The coated sample was designated as D-NCM811.

2.2 Wet coating method

The wet coating process began by adding 20 g of NCM811 cathode material and an appropriate amount of $Al(NO_3)_3{\cdot}9H_2O$ coating material to 20 mL of deionized (D.I) water. The mixture was stirred for 20 min. Next, to evaporate the solvent, the mixture was dried in a convection oven at 120°C for 2 h. Subsequently, it was further dried in a vacuum oven at 120°C for another 2 h. After vacuum drying, the sample was calcined in a box furnace at 700°C for 6 h under an O_2 atmosphere. The final material obtained through this process, Al_2O_3 wet-coated NCM811, was designated as W-NCM811.

2.3 Material characterization

To analyze the crystal structure of the coated cathode materials, an X-ray diffractometer (XRD, Bruker) equipped with Cu Kα radiation was used under a scanning range of 5°–90°. The surface morphology of the cathode materials and the distribution of the Al coating layer were analyzed using a Field Emission Scanning Electron Microscope (FE-SEM, JSM-7600F) operated at 15 kV. Additionally, the elemental morphology on the cathode surface was examined *via* Energy Dispersive X-ray Spectroscopy (EDS). For analyzing the thickness of the surface coating layer on the coated samples, a High-Resolution Transmission Electron Microscope (HR-TEM, JEM ARM 200F) was used. X-ray Photoelectron Spectroscopy (XPS, ESCALAB250) was performed to examine the chemical state of the surface using an Al anode as the X-ray source. The energy level was calibrated based on the C-C peak of Carbon 1s set at 285 eV. To confirm whether the coating amount was effectively controlled depending on the coating method, the concentrations of metallic elements were measured using an inductively coupled plasma-optical emission spectrometer (ICP-OES).

2.4 Electrochemical characterization

Cathode composite electrode was prepared with a mass ratio of 96:2:2, consisting of NCM811 active material, carbon black conductive additive, and polyvinylidene fluoride (PVdF, KF-1100) binder. The active material, conductive additive, and binder were first ground and mixed, and then N-methyl-2-pyrrolidone (NMP, Sigma-Aldrich) solvent was added to form a slurry. The prepared electrode slurry was coated onto an Al foil current collector. The electrode thickness was designed to achieve a capacity of 1 mAh cm^{-2}. The coated electrode was dried in a convection oven at 120°C for 10 min to remove the NMP solvent. Subsequently, a roll-press process was performed to enhance the adhesion between the active material and the current collector while achieving a smooth and uniform electrode surface with consistent thickness. The completed electrode was punched into circular shapes with a diameter of 1.2 cm for use in coin type half cells. The circular electrodes were dried in a vacuum oven at 120°C for 10 h to ensure complete removal of moisture. A coin cell (2032-type) was assembled inside an argon (Ar) atmosphere glove box, using the circular electrode as the cathode and Li metal as the anode and counter electrode to fabricate a half-cell. A polypropylene (PP) separator was used, and the electrolyte consisted of a 1 M $LiPF_6$ solution in a mixture of ethylenecarbonate (EC) and diethylcarbonate (DEC) at a 1:1 volume ratio. All electrochemical analyses were conducted at the controlled room temperature (25°C). The galvanostatic cycling test was carried out using a battery testing system (Won-A-Tech, South Korea) within a potential window of 2.5–4.3 V. Electrochemical impedance spectroscopy (EIS) analysis was performed after charging the samples to 4.3 V to ensure the same state of charge (SOC) among them. After reaching 4.3 V, the cells were charged under constant voltage conditions until the current density stabilized below 0.05 C. To achieve a stable open circuit voltage (OCV), the cells were allowed to stabilize for 1 h. EIS measurements were then conducted over a frequency range of 0.01–100 kHz with an amplitude of 5 mV.

3 Results and discussion

TGA analysis was conducted to determine the coating temperature for $Al(NO_3)_3{\cdot}9H_2O$. Supplementary Figure S1 shows the TGA curve of $Al(NO_3)_3{\cdot}9H_2O$ under an O_2 atmosphere. As observed in Supplementary Figure S1, no further weight loss occurs beyond 400°C. Therefore, temperatures of 400°C and 700°C were selected for the coating process. This is because Al_2O_3 is formed at 400°C, and at 700°C, it reacts with Li to form $LiAlO_2$ (Li L. et al., 2018). As shown in Supplementary Figure S2, the results indicate that 700°C demonstrates improved electrochemical performance. Additionally, a comparison of Al_2O_3 coating contents at 0.1, 0.5 and 1wt%, respectively, as seen in Supplementary Figure S3, that 0.5wt% exhibits enhanced electrochemical performance. Therefore, 0.5wt% was selected as the coating content for both dry and wet coating methods, and the process was carried out at 700°C.

XRD pattern analysis was conducted to examine whether the dry and wet Al_2O_3 coatings affected the crystal structure of NCM811. As shown in the XRD patterns in Figure 1A, both bare NCM811 and coated NCM811 correspond to α-$NaFeO_2$ layered structure (*R3m* lattice space group, JCPDS card No. 82–1,495) (Yang et al., 2024). The distinct peak splitting of (006)/(102) and (108)/(110) peaks in all samples had indicated that the layered structure of the material had been well-developed (Sim et al., 2020). The ratio $I_{(003)}/I_{(104)}$ had served as an indicator of the degree of cation mixing in layered structures, where a higher value had been preferred (Sim et al., 2020). Moreover, it had been reported that, due to the similarity in ionic radii between Li^+ (0.76 Å) and Ni^{2+} (0.69 Å), these ions had migrated from 3a sites to 3b sites, and a value below 1.2 had indicated severe cation mixing (Weber et al., 2020). The values for bare NCM811, D-NCM811, and W-NCM811 were 1.92, 1.94, and 1.96, respectively, showing similar results, which had suggested that the extent of cation mixing had been comparable across all samples. Additionally, due to the low content of Al_2O_3 after coating, peaks for Al_2O_3 had not been observed in the XRD patterns (Li L. et al., 2018). However, as shown in Figure 1B, the dry coated sample exhibited a shift to the left after coating. This shift had potentially been attributed to the expansion of the interlayer spacing (c-axis direction) that had been caused by changes in the oxygen arrangement following the loss of Li ions at the surface, and this behavior could also be associated with the formation of a small amount of $LiAlO_2$ during the coating process (Li L. et al., 2018).

The effects of the coating process on the particles were examined using FE-SEM. Figures 2A–C shows the secondary particles of bare NCM811, D-NCM811, and W-NCM811, respectively, while Figures 2D–I present the Ni and Al element EDS mapping for each sample. The images reveal no significant changes in the particle morphology before and after coating. Additionally, as confirmed by the EDS mapping, the uniform distribution of Al demonstrates that the coating layer was uniformly applied. The size of the secondary particles for all samples was approximately 20 μm.

HR-TEM analysis was conducted to confirm the coating layer. Figures 3A–C shows the images of bare NCM811, D-NCM811, and

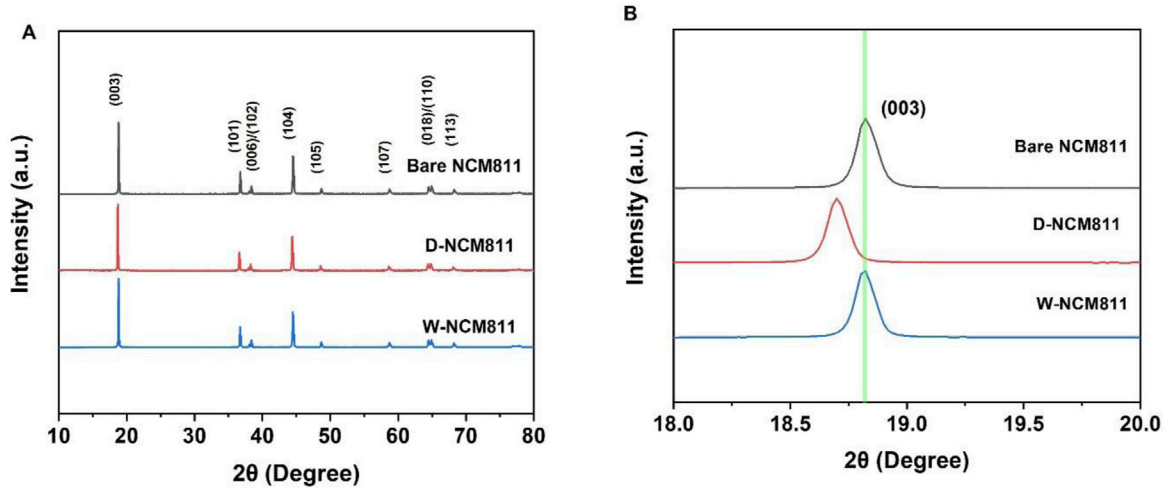

FIGURE 1
(A) XRD patterns of bare NCM811, D-NCM811 and W-NCM811; **(B)** enlarged view of the (003) peak.

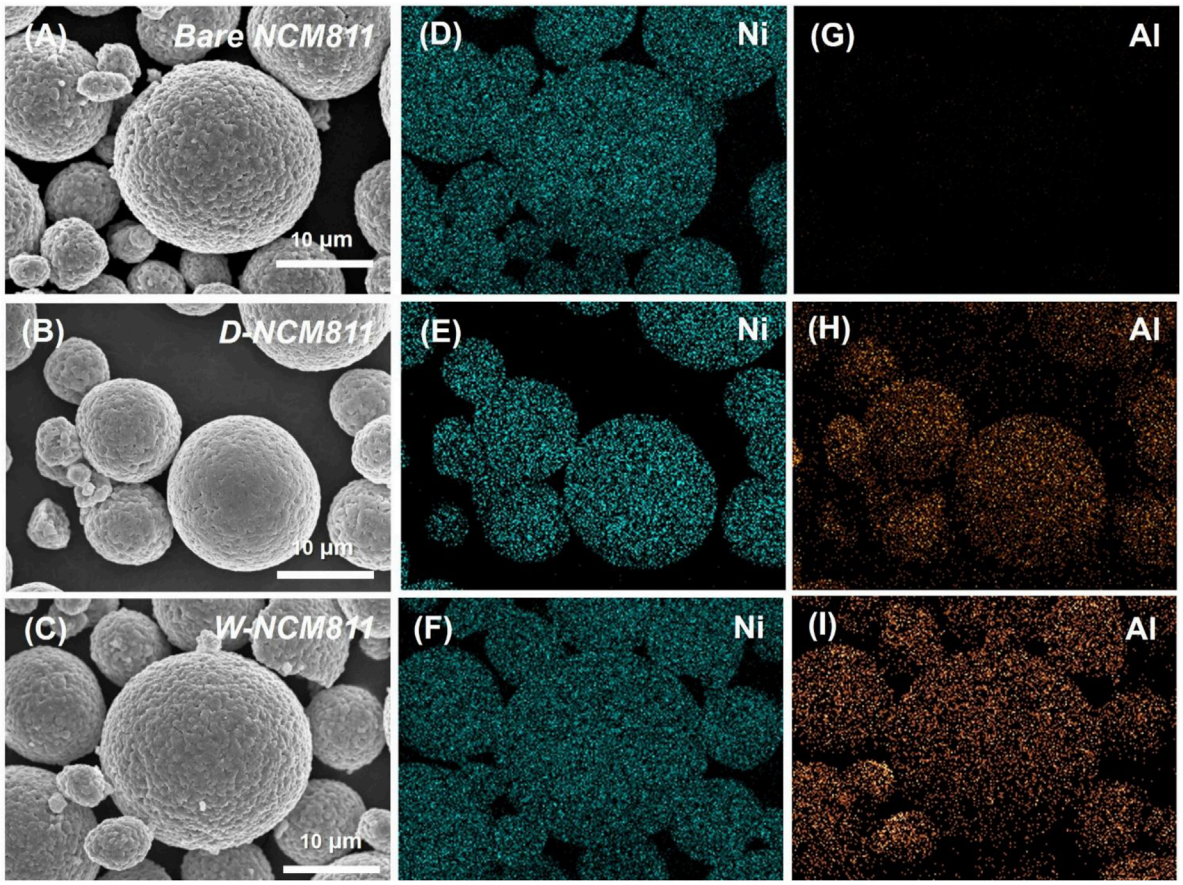

FIGURE 2
FE-SEM image of **(A)** bare NCM811, **(B)** D-NCM811 and **(C)** W-NCM811; EDS mapping of **(D–F)** Ni element of bare NCM811, D-NCM811 and W-NCM811; **(G–I)** Al element of bare NCM811, D-NCM811 and W-NCM811.

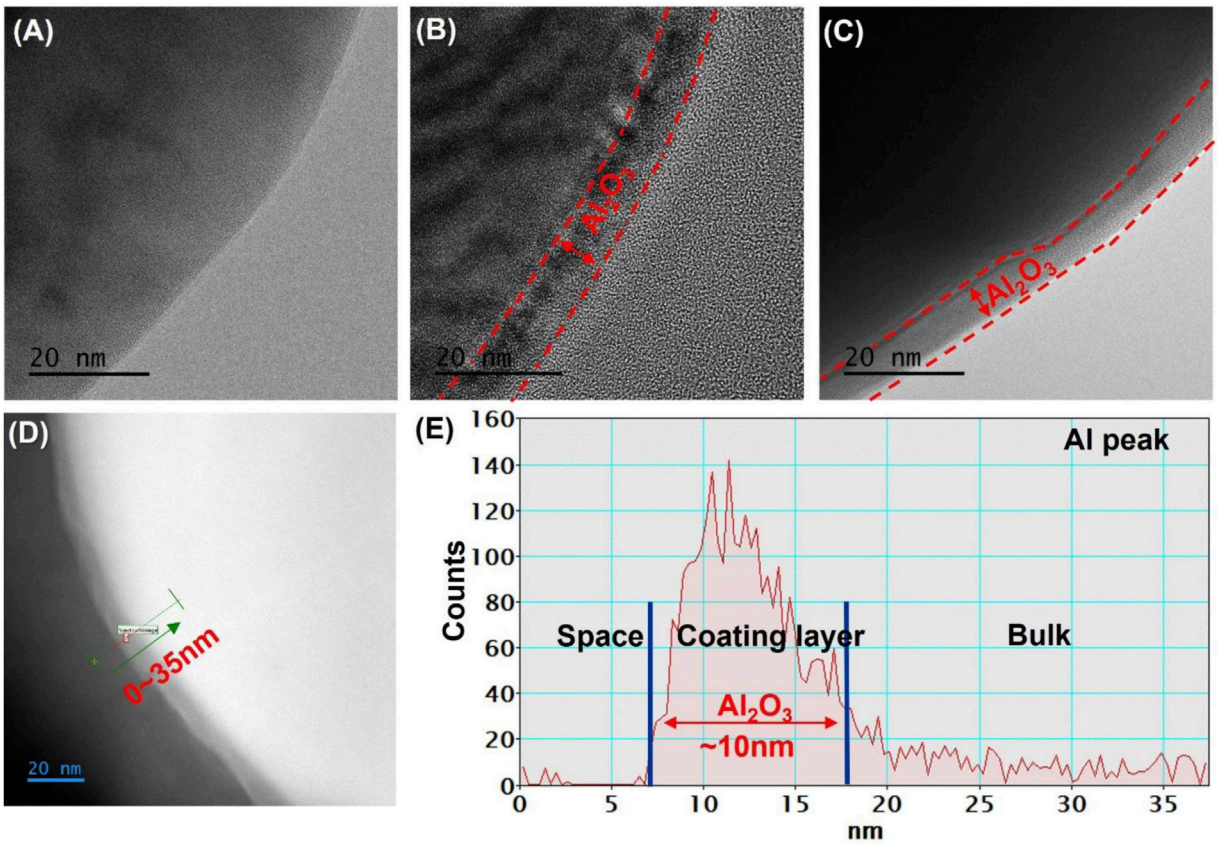

FIGURE 3
HR-TEM image of **(A)** bare NCM811, **(B)** D-NCM811 and **(C)** W-NCM811; **(D,E)** ADF of D-NCM811 Al line scan.

TABLE 1 Chemical compositions of lithiated oxide powders determined by ICP-OES.

Sample	Chemical composition			
	Ni (At%)	Co (At%)	Mn (At%)	Al (At%)
Bare	79.56	10.26	10.18	-
D-NCM811	79.11	10.00	10.12	0.77
W-NCM811	79.20	9.93	10.09	0.78

W-NCM811, respectively. The HR-TEM images in Figure 3B, C show that the Al_2O_3 coating layer exhibited similar morphology and thickness, independent of the coating method. HR-TEM analysis in ADF mode was conducted, and the EDS line scan results are shown in Figure 3D, with the corresponding Al peak illustrated in Figure 3E. The Al_2O_3 coating layer analysis revealed that no Al peaks were present in uncoated regions, whereas significant Al peaks were observed in the coating layer regions. The results indicate that the Al_2O_3 coating layer was formed with a thickness of approximately 10 nm.

ICP-OES analysis was conducted, and the results are presented in Table 1 to determine the Al atomic percentage across the active material. The Al atomic percentages for D-NCM811 and W-NCM811 were determined to be 0.77% and 0.78%, respectively, showing nearly identical values. These results are consistent with HR-TEM observations, which also revealed that the thickness and morphology of the coating layers for both samples were comparable.

XPS surface analysis was used to determine the Ni^{2+} ratios, as shown in Figures 4A–C. The Ni^{2+} ratios for bare NCM811, D-NCM811, and W-NCM811 were measured to be 19.3, 18.2, and 33.7%, respectively. The Ni^{2+} ratio in D-NCM811, prepared *via* the dry coating method, showed minimal change, whereas the ratio in W-NCM811 significantly increased following the wet coating method. This result demonstrates that wet processing conditions, even without coating (Wet-W/O coating), lead to a substantial increase in the NiO-like phase on the NCM811 surface, as shown in Figure 4D (Zhang, 2020). The electrochemically inactive NiO-like phase formed on the NCM811 surface acts as a resistive layer, hindering Li-ion diffusion (Ivanishchev et al., 2023). The formation of this resistive NiO-like phase likely caused the increased resistance components observed during the earlier cycle ability evaluation. This was further exacerbated by the resulting cation mixing (Cui et al., 2021). Figure 4E presents the Al 2p spectra. Analysis of NCM811 after both dry and wet coating processes confirmed the formation of $LiAlO_2$ in the dry coated sample (Liu et al., 2018). This formation is attributed to the additional reaction between Li residues distributed on the surface of NCM811 and the coated Al_2O_3. The observed result aligns well with the peak shifting identified in the XRD analysis. According to reported studies,

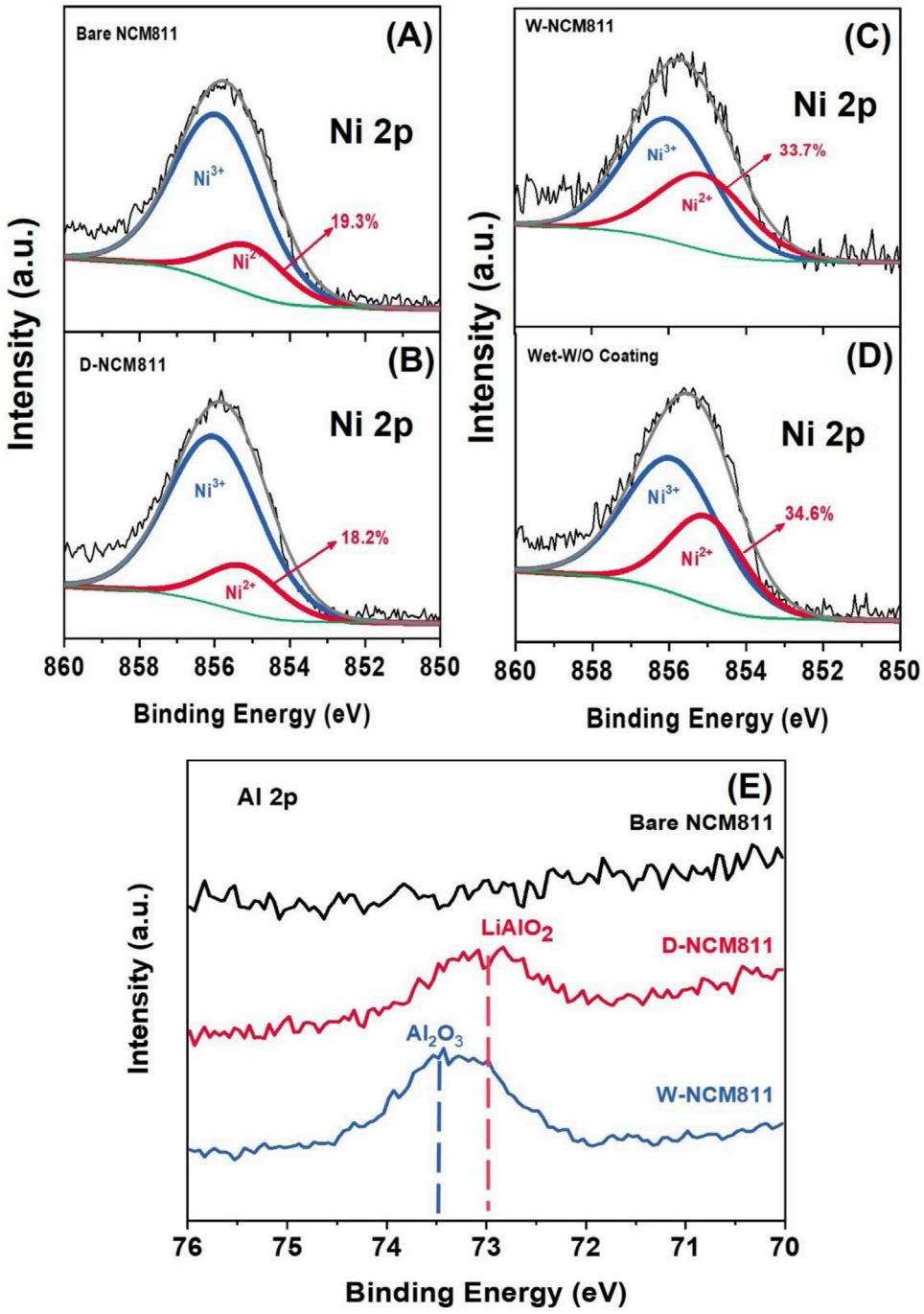

FIGURE 4
XPS Ni 2p spectra of **(A)** bare NCM811, **(B)** D-NCM811, **(C)** W-NCM811 and **(D)** wet condition without coating; **(E)** Al 2p spectra of all samples.

$LiAlO_2$ is known to enhance electrochemical conductivity (Liu et al., 2018). These findings suggest that the dry coating process contributes to improving the electrochemical performance of Ni-rich cathode materials.

Electrochemical analyses were conducted to evaluate the effects of different coating methods. Figures 5A–C illustrates the galvanostatic charge-discharge voltage profiles for bare NCM811, D-NCM811, and W-NCM811 at a 0.1C for the 1st cycle and at a 0.5C from the 2nd to the 150th cycles. The initial charge and discharge capacities at a 0.1C were 229.0, 227.9, and 224.6 mAh g^{-1} and 197.0, 197.4, and 194.6 mAh g^{-1} for bare NCM811, D-NCM811, and W-NCM811, respectively. The corresponding initial Coulombic efficiencies were 86.0%, 86.6%, and 86.5%. These results suggest that both dry and wet coating methods mitigate initial electrolyte side reactions. Figure 5D shows the cycling performance at 0.5C from the 2nd to the 150th cycles. The retention rates for bare NCM811, D-NCM811, and W-NCM811 were 78.1%, 84.3%, and 77.4%, respectively, while

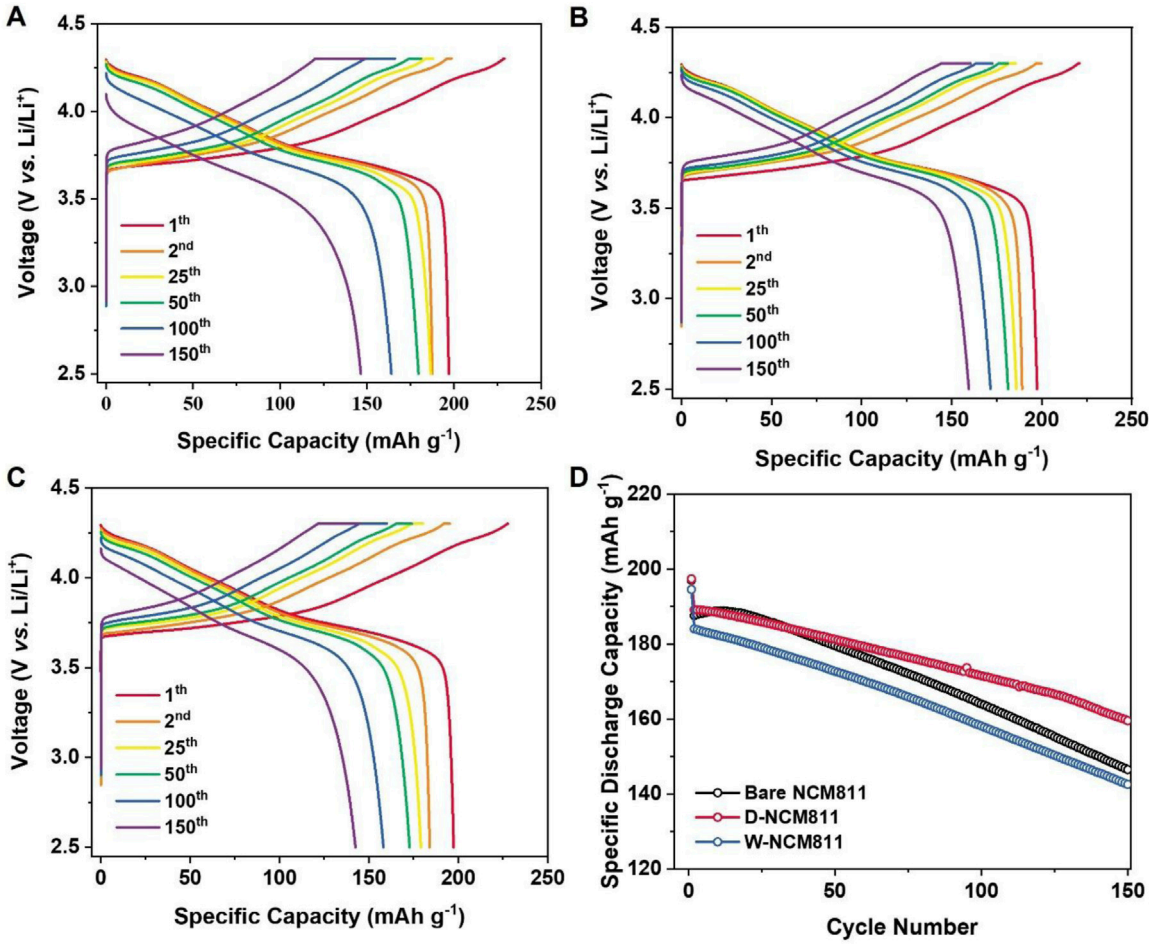

FIGURE 5
Galvanic charge/discharge curve of cycled from 2.5 to 4.3 V at 25°C. And the initial cycle is 0.1C rate and after 0.5C rate of **(A)** bare NCM811, **(B)** D-NCM811 and **(C)** W-NCM811; **(D)** Cycling performance at initial 0.1 C rate and after 0.5C rate of all samples.

the corresponding average Coulombic efficiencies were 98.9%, 99.3%, and 99.0%. Furthermore, as observed in the discharge voltage curves in Figures 5A–C, the overpotentials increased with the number of cycles in the order of bare NCM811, D-NCM811, and W-NCM811. These results confirm, consistent with previous findings, that D-NCM811 effectively suppressed both initial electrolyte side reactions and surface degradation during cycling. In contrast, W-NCM811 exhibited lower overpotential increases compared to bare NCM811. The instability of W-NCM811, caused by the formation of a NiO-like phase, leads to a degradation in cycle characteristics.

The rate performance evaluation was conducted by two sequences. In the first stage, as shown in Figure 6A, each C-rate from 0.1 to 20 C was tested for 3 cycles. In the second stage, after 150 cycles at a 0.5 C-rate, the rate performance was re-evaluated by testing each C-rate from 0.1 to 10 C for three cycles, as illustrated in Figure 6B. This method reflects the operation rate of LIBs in the application under repeating cycling. The first-stage rate performance evaluation showed that the performance decreased in the order of bare NCM811 > D-NCM811 > W-NCM811. This result indicates that, during the first-stage rate performance test, the interfacial resistance caused by the Al_2O_3 and $LiAlO_2$ coating layer was greater than the resistance caused by side reactions with the electrolyte. Therefore, bare NCM811 exhibited better rate characteristics compared to D-NCM811. For W-NCM811, the NiO-like phase formed during the coating process introduced additional resistance, leading to greater capacity loss compared to both bare NCM811 and D-NCM811. To evaluate the rate performance after substantial cell degradation, further assessments were conducted following the 150th cycle, as shown in Figure 6B. This stage was designed to investigate the impact of the thick SEI layer and cation mixing on battery performance. Unlike the first stage, D-NCM811 demonstrated the highest discharge capacity under high-rate conditions after prolonged cycling, particularly at 5C. This shows that the interfacial resistance initially increased due to the coating layer formed by Al_2O_3 and $LiAlO_2$ on the surface of NCM811. However, after 150 cycles, the stabilized CEI layer and the formation of Al_2O_3 and $LiAlO_2$ demonstrate higher performance. Furthermore, the discharge capacities of bare NCM811 and W-NCM811 were similar. These differences were most noticeable in Figure 6C. This suggests that their reduced discharge capacities under high-rate cycling from distinct degradation mechanisms: electrolyte side reactions dominated in bare NCM811, whereas NiO-like phase formation and cation mixing were predominant in W-NCM811 (Zhang, 2020). In contrast, D-NCM811

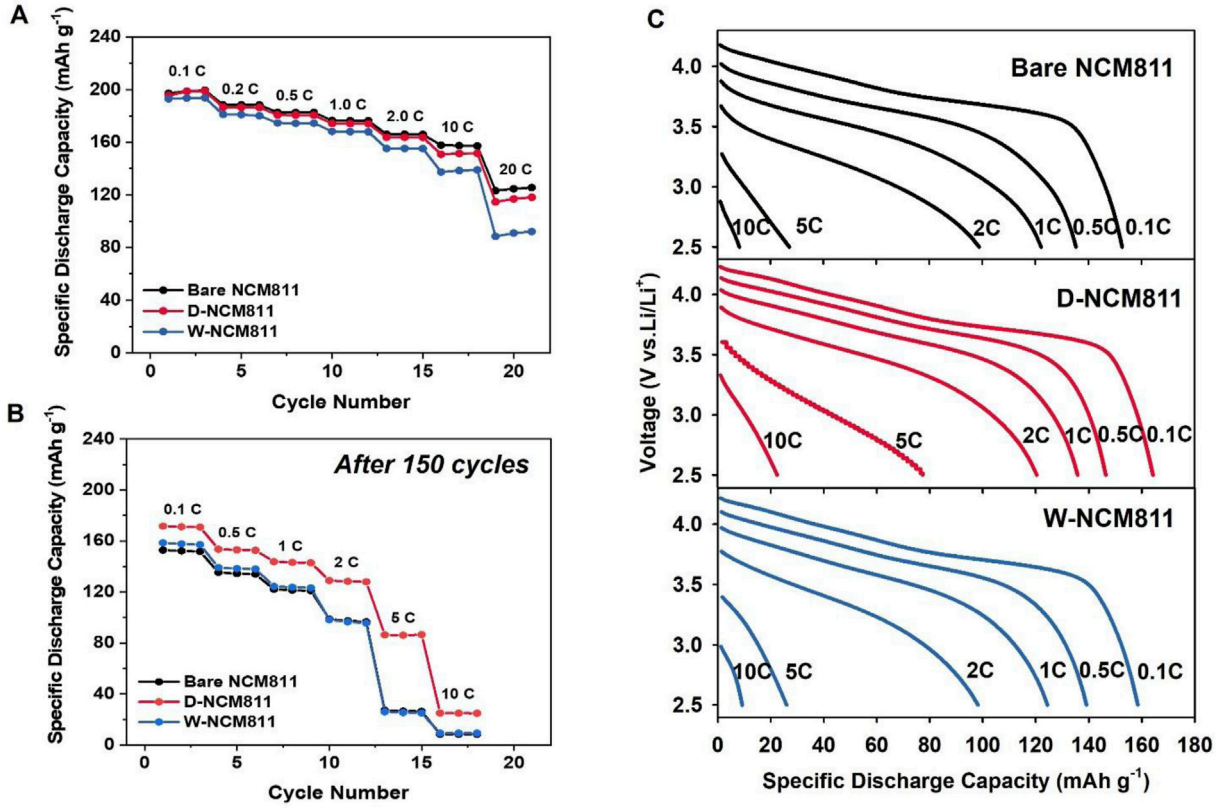

FIGURE 6
Galvanic charge/discharge curve of cycled from 2.5 to 4.3 V at 25°C. **(A)** Rate capability; **(B)** after 150 cycles of rate capability; **(C)** after 150 cycles of galvanic discharge rate performance of bare NCM811, D-NCM811 and W-NCM811.

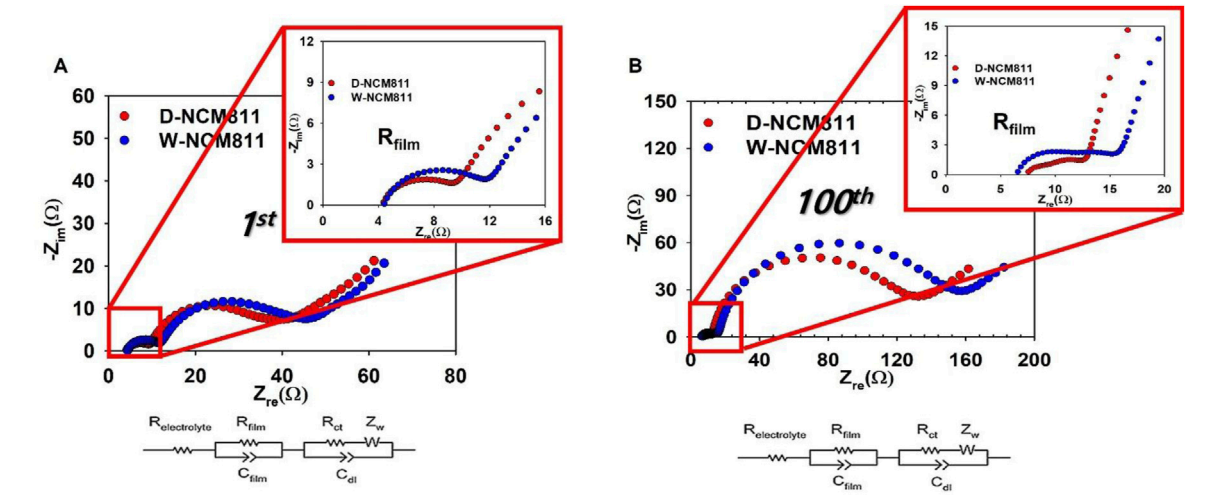

FIGURE 7
EIS Nyquist plots of the 1st cycle **(A)** and the 100th cycle **(B)** for D-NCM811 and W-NCM811.

effectively suppressed reactions with the electrolyte, achieving higher discharge capacities even under high-rate conditions. These findings indicate that the dry coating method applied to D-NCM811 was more effective in mitigating degradation phenomena such as resistance increase from side reactions and cation mixing. These issues were prevalent in bare NCM811 and W-NCM811, respectively. As a result, D-NCM811 exhibited superior rate performance after prolonged cycling degradation.

TABLE 2 EIS fitting data of the D-NCM811 and W-NCM811.

Samples	R_{film} (1st) (Ω)	R_{film} (100th) (Ω)	R_{ct} (1st) (Ω)	R_{ct} (100th) (Ω)
D-NCM811	5.0	8.7	37.63	130.06
W-NCM811	7.8	17.7	45.86	155.49

Finally, EIS analysis was conducted on cells with D-NCM811 and W-NCM811 to investigate resistance components, focusing on surface resistance (R_{film}) and charge transfer resistance (R_{ct}) observed in Nyquist plots after charging the cells to 4.3 V *versus* Li/Li^+ (Ivanishchev et al., 2023). Figure 7A presents the EIS results from the 1st cycle, where both the first semicircle resistance (R_{film}) and the second semicircle resistance (R_{ct}) for D-NCM811 were observed to be smaller than those for W-NCM811 (Liang et al., 2015). As shown in the results presented in Table 2, the R_{film} and R_{ct} values were 5.0 and 37.63 Ω for D-NCM811 and 7.8 and 45.86 Ω for W-NCM811. This result indicates that the higher R_{film} and R_{ct} values in W-NCM811 are directly correlated with its lower capacity retention, highlighting the importance of interfacial stability in achieving long-term performance (Strehle et al., 2021). The greater R_{film} and R_{ct} values in W-NCM811 after the first charge can be attributed to the NiO-like phase formed on its surface, which contributes significantly to interfacial resistance. Additionally, as shown in Figure 7B, EIS results after the 100th cycle revealed that both R_{film} and R_{ct} exhibited more pronounced differences compared to their initial values. According to the results listed in Table 2, the R_{film} and R_{ct} values were 8.7 and 130.06 Ω for D-NCM811 and 17.7 Ω and 155.49 for W-NCM811. In D-NCM811, the Al_2O_3 and $LiAlO_2$ coating layers effectively suppressed side reactions with the electrolyte, thereby preventing a significant increase in surface resistance over time. In contrast, W-NCM811 displayed a notable increase in resistance attributed to the pre-formed NiO-like phase on its surface as well as additional resistance from cation mixing during cycling. The lower R_{ct} observed in D-NCM811 suggests that the Al_2O_3 and $LiAlO_2$ coating promotes Li^+ transport by providing a uniform ion-conductive pathway, whereas the NiO-like phase in W-NCM811 acts as a kinetic barrier, hindering Li^+ transport (Wang et al., 2023). These observations emphasize the effectiveness of the Al_2O_3 coating in mitigating degradation in D-NCM811, while highlighting the detrimental effects of the NiO-like phase and cation mixing on the resistance and performance of W-NCM811 (Hu et al., 2021).

4 Conclusion

Ni-rich cathode materials exhibit high theoretical capacities but face challenges such as surface instability and significant capacity fading, primarily due to the high reactivity of Ni. This study investigates and compares the effects of dry and wet coating processes on the structural and electrochemical properties of these materials. The wet coating process uses deionized water, while the dry coating process involves high-speed mixing. XRD analysis reveals no distinct peaks for Al_2O_3 or $LiAlO_2$ in D-NCM811, suggesting that these phases are formed only in small quantities through a reaction between surface lithium and Al_2O_3 without significantly altering the structure. In contrast, no such reactions or changes are observed in NCM811 or W-NCM811. SEM and TEM analyses confirm that the particle morphology remains largely unchanged, while ICP analysis shows aluminum levels of 77% and 78% for dry and wet coatings, respectively. XPS analysis indicates that the Ni^{3+}/Ni^{2+} ratio is lowest in dry coating, while wet coating results in an excessive presence of Ni^{2+} due to the formation of a NiO-like phase. Moreover, Al bonding analysis reveals signatures consistent with Al_2O_3 or $LiAlO_2$ after dry coating, corroborating the XRD results and confirming the limited formation of these phases. Electrochemical tests reveal that the initial discharge capacities at a 0.1C rate for NCM811, W-NCM811, and D-NCM811 are 197.0, 197.4, and 194.6 mAh g^{-1}, respectively, with retention rates of 78.1%, 84.3%, and 77.4% after 150 cycles at a 0.5C rate. While the first phase rate performance of D-NCM811 is initially lower than that of bare NCM811, its second phase performance after 150 cycles surpasses others, particularly at 0.5C, due to the Al_2O_3 and $LiAlO_2$ improving conductivity and providing a stable surface layer over time. In contrast, W-NCM811 displays lower performance caused by structural degradation and instability due to the formation of the NiO-like phase. The EIS results further support these findings, showing smaller interfacial resistance arcs for D-NCM811 compared to W-NCM811 across cycles. These results demonstrate that the dry coating process provides significant advantages over the wet coating process by enhancing the long-term stability and electrochemical performance of Ni-rich cathode materials. However, challenges such as achieving coating uniformity and scalability in large-scale manufacturing remain and should be addressed in future research. Nevertheless, this study underscores the critical importance of surface coating technologies in addressing persistent issues of Ni-rich cathodes and highlights the dry coating process as a promising approach for realizing high-performance and durable batteries.

Data availability statement

The raw data supporting the conclusions of this article will be made available by the authors, without undue reservation.

Author contributions

KL: Data curation, Formal Analysis, Investigation, Methodology, Visualization, Writing – original draft. FJ: Data curation, Visualization, Writing – original draft. SJ: Investigation, Supervision, Validation, Writing – review and editing. HL: Data curation, Investigation, Writing – review and editing. JK: Conceptualization, Investigation, Writing – review and editing. JM: Conceptualization, Funding acquisition, Investigation, Writing – original draft, Writing – review and editing.

Funding

The author(s) declare that financial support was received for the research and/or publication of this article. This work was supported

by the Ministry of Trade, Industry and Energy/Korea Evaluation Institute of Industrial Technology (MOTIE/KEIT) (No. 20022514).

Conflict of interest

The authors declare that the research was conducted in the absence of any commercial or financial relationships that could be construed as a potential conflict of interest.

Generative AI statement

The author(s) declare that no Generative AI was used in the creation of this manuscript.

Publisher's note

Supplementary material

The Supplementary Material for this article can be found online at: https://www.frontiersin.org/articles/10.3389/fbael.2025.1647877/full#supplementary-material

References

Cui, J., Ding, X., Luo, D., Xie, H., Zhang, Z., Zhang, B., et al. (2021). Effect of cationic uniformity in precursors on Li/Ni mixing of Ni-Rich layered cathodes. *Energy and Fuels* 35, 1842–1850. doi:10.1021/acs.energyfuels.0c03967

Han, B., Paulauskas, T., Key, B., Peebles, C., Park, J. S., Klie, R. F., et al. (2017). Understanding the role of temperature and cathode composition on interface and bulk: optimizing aluminum oxide coatings for Li-Ion cathodes. *ACS Appl. Mater Interfaces* 9, 14769–14778. doi:10.1021/acsami.7b00595

Hartmann, L., Pritzl, D., Beyer, H., and Gasteiger, H. A. (2021). Evidence for li $^{+}$/H $^{+}$ exchange during ambient storage of Ni-Rich cathode active materials. *J. Electrochem Soc.* 168, 070507. doi:10.1149/1945-7111/ac0d3a

Herzog, M. J., Gauquelin, N., Esken, D., Verbeeck, J., and Janek, J. (2021). Facile dry coating method of high-nickel cathode material by nanostructured fumed alumina (al $_2$ O $_3$) improving the performance of lithium-ion batteries. *Energy Technol.* 9. doi:10.1002/ente.202100028

Ho, V.-C., Huynh, T. N., Pham, T. H., Kim, H., Jung, H.-G., Kim, K. J., et al. (2025b). Dry basal plane graphene wrappings on spherical nickel-rich oxide layered particles for lithium-ion batteries. *J. Energy Chem.* 104, 10–19. doi:10.1016/j.jechem.2024.12.020

Ho, V.-C., Huynh, T. N., Jung, H.-G., Kim, J. H., Oh, S.-M., Kim, Y.-J., et al. (2025a). Dry carbon nanotube wrapping of Ni-rich layered oxide cathodes for lithium-ion batteries. *Sustain. Mater. Technol.* 43, e01287. doi:10.1016/j.susmat.2025.e01287

Hong, M., Ho, V.-C., and Mun, J. (2024). Comprehensive review of single-crystal Ni-rich cathodes: single-crystal synthesis and performance enhancement strategies. *Front. Batter. Electrochem.* 3. doi:10.3389/fbael.2024.1338069

Hong, M., Lee, S., Ho, V.-C., Lee, D., Yu, S.-H., and Mun, J. (2022). Unraveling the dynamic interfacial behavior of LiCoO $_2$ at various voltages with lithium bis(oxalato) borate for lithium-ion batteries. *ACS Appl. Mater Interfaces* 14, 10267–10276. doi:10.1021/acsami.1c21952

Hu, D., Du, F., Cao, H., Zhou, Q., Sun, P., Xu, T., et al. (2021). An effective strategy to control thickness of Al2O3 coating layer on nickel-rich cathode materials. *J. Electroanal. Chem.* 880, 114910. doi:10.1016/j.jelechem.2020.114910

Ivanishchev, A. V., Lee, S.-H., Kim, J.-J., Ivanishcheva, I. A., Nam, S.-C., and Song, J.-H. (2023). Li-ion diffusion characteristics of surface modified Ni-rich NCM cathode material. *J. Electroanal. Chem.* 932, 117242. doi:10.1016/j.jelechem.2023.117242

Jeong, S., Choi, K., Ho, V.-C., Cho, J., Bae, J.-S., Nam, S. C., et al. (2022). Crucial role of Ni-doping to interfacial Li2MnO3 layer of high-performance Ni-rich layered cathode in lithium-ion batteries. *Chem. Eng. J.* 434, 134577. doi:10.1016/j.cej.2022.134577

Kalluri, S., Yoon, M., Jo, M., Liu, H. K., Dou, S. X., Cho, J., et al. (2017). Feasibility of cathode surface coating technology for high-energy lithium-ion and beyond-lithium-Ion batteries. *Adv. Mater.* 29. doi:10.1002/adma.201605807

Kasnatscheew, J., Evertz, M., Streipert, B., Wagner, R., Nowak, S., Cekic Laskovic, I., et al. (2017). Changing established belief on capacity fade mechanisms: thorough investigation of LiNi $_{1/3}$ Co $_{1/3}$ Mn $_{1/3}$ O $_2$ (NCM111) under high voltage conditions. *J. Phys. Chem. C* 121, 1521–1529. doi:10.1021/acs.jpcc.6b11746

Li, L., Zhang, Z., Fu, S., Liu, Z., and Liu, Y. (2018a). Co-modification by LiAlO2-coating and Al-doping for LiNi0.5Co0.2Mn0.3O2 as a high-performance cathode material for lithium-ion batteries with a high cutoff voltage. *J. Alloys Compd.* 768, 582–590. doi:10.1016/j.jallcom.2018.07.223

Li, M., Lu, J., Chen, Z., and Amine, K. (2018b). 30 years of lithium-ion batteries. *Adv. Mater.* 30, e1800561. doi:10.1002/adma.201800561

Liang, C., Liu, L., Jia, Z., Dai, C., and Xiong, Y. (2015). Synergy of nyquist and bode electrochemical impedance spectroscopy studies to particle size effect on the electrochemical properties of LiNi0.5Co0.2Mn0.3O2. *Electrochimica Acta* 186, 413–419. doi:10.1016/j.electacta.2015.10.190

Liu, C., Neale, Z. G., and Cao, G. (2016). Understanding electrochemical potentials of cathode materials in rechargeable batteries. *Mater. Today* 19, 109–123. doi:10.1016/j.mattod.2015.10.009

Liu, W., Li, X., Xiong, D., Hao, Y., Li, J., Kou, H., et al. (2018). Significantly improving cycling performance of cathodes in lithium ion batteries: the effect of Al2O3 and LiAlO2 coatings on LiNi0.6Co0.2Mn0.2O2. *Nano Energy* 44, 111–120. doi:10.1016/j.nanoen.2017.11.010

Ma, J., Huang, X., Huang, R., Tang, Y., Huang, S., Wang, Y., et al. (2025). An ultra-high nickel cobalt-free cathode material toward high-energy and long-cycle stable Li-ion batteries: a single-crystal and surface high-entropy design strategy. *J. Mater. Chem. A* 13, 15858–15870. doi:10.1039/D5TA01897H

Mitra, S., and Sudakar, C. (2024). High rate capability and cyclic stability of Ni-rich layered oxide LiNi $_{0.83}$ Co $_{0.12}$ Mn $_{0.05-x}$ Al $_x$ O $_2$ cathodes: nanofiber *versus* nanoparticle morphology. *Battery Energy* 3. doi:10.1002/bte2.20230066

Mun, J., Yim, T., Park, J. H., Ryu, J. H., Lee, S. Y., Kim, Y. G., et al. (2014). Allylic ionic liquid electrolyte-assisted electrochemical surface passivation of LiCoO2 for advanced, safe lithium-ion batteries. *Sci. Rep.* 4, 5802. doi:10.1038/srep05802

Nitta, N., Wu, F., Lee, J. T., and Yushin, G. (2015). Li-ion battery materials: present and future. *Mater. Today* 18, 252–264. doi:10.1016/j.mattod.2014.10.040

Park, H. G., Min, K., and Park, K. (2022). A synergistic effect of Na $^{+}$ and Al $^{3+}$ dual doping on electrochemical performance and structural stability of LiNi $_{0.88}$ Co $_{0.08}$ Mn $_{0.04}$ O $_2$ cathodes for Li-Ion batteries. *ACS Appl. Mater Interfaces* 14, 5168–5176. doi:10.1021/acsami.1c16042

Qu, X., Huang, H., Wan, T., Hu, L., Yu, Z., Liu, Y., et al. (2022). An integrated surface coating strategy to enhance the electrochemical performance of nickel-rich layered cathodes. *Nano Energy* 91, 106665. doi:10.1016/j.nanoen.2021.106665

Roy, J. J., Phuong, D. M., Verma, V., Chaudhary, R., Carboni, M., Meyer, D., et al. (2024). Direct recycling of li-ion batteries from cell to pack level: challenges and prospects on technology, scalability, sustainability, and economics. *Carbon Energy* 6. doi:10.1002/cey2.492

Sim, S.-J., Lee, S.-H., Jin, B.-S., and Kim, H.-S. (2020). Use of carbon coating on LiNi0.8Co0.1Mn0.1O2 cathode material for enhanced performances of lithium-ion batteries. *Sci. Rep.* 10, 11114. doi:10.1038/s41598-020-67818-5

Sim, Y. B., Lee, H., Mun, J., and Kim, K. J. (2024). Modification strategies improving the electrochemical and structural stability of high-Ni cathode materials. *J. Energy Chem.* 96, 185–205. doi:10.1016/j.jechem.2024.04.029

Strehle, B., Friedrich, F., and Gasteiger, H. A. (2021). A comparative study of structural changes during long-term cycling of NCM-811 at ambient and elevated temperatures. *J. Electrochem Soc.* 168, 050512. doi:10.1149/1945-7111/abf780

Sun, H. H., Kim, U.-H., Park, J.-H., Park, S.-W., Seo, D.-H., Heller, A., et al. (2021). Transition metal-doped Ni-rich layered cathode materials for durable Li-ion batteries. *Nat. Commun.* 12, 6552. doi:10.1038/s41467-021-26815-6

Wang, F., Liang, W., Liu, K., Zhao, Y., Shi, L., Wang, Z., et al. (2024a). Surface atomic arrangement of primary particles through pre-oxidation to enhance the performance of LiNi0.8Co0.1Mn0.1O2 cathode materials. *Chem. Eng. J.* 495, 153503. doi:10.1016/j.cej.2024.153503

Wang, J., Zhao, D., Zhou, G., Wei, S., Hou, S., Li, Y., et al. (2023). Effects of Al2O3 and LiAlO2 Co-coating on electrochemical properties of LiNi0.8Co0.1Mn0.1O2 cathode materials. *Ceram. Int.* 49, 15842–15850. doi:10.1016/j.ceramint.2023.01.179

Wang, W., Xiao, Z., Liu, J., He, X., Wen, J., Zhou, Y., et al. (2024b). Surface atomic rearrangement with high cation ordering for ultra-stable single-crystal ni-rich co-less cathode materials. *Adv. Funct. Mater.* 34, 2409956. doi:10.1002/adfm.202409956

Weber, D., Tripković, Đ., Kretschmer, K., Bianchini, M., and Brezesinski, T. (2020). Surface modification strategies for improving the cycling performance of ni-rich cathode materials. *Eur. J. Inorg. Chem.* 2020, 3117–3130. doi:10.1002/ejic.202000408

Yan, J., Huang, H., Tong, J., Li, W., Liu, X., Zhang, H., et al. (2022). Recent progress on the modification of high nickel content NCM: coating, doping, and single crystallization. *Interdiscip. Mater.* 1, 330–353. doi:10.1002/idm2.12043

Yang, T., Luo, D., Zhang, X., Gao, S., Gao, R., Ma, Q., et al. (2024). Sustainable regeneration of spent cathodes for lithium-ion and post-lithium-ion batteries. *Nat. Sustain* 7, 776–785. doi:10.1038/s41893-024-01351-5

Zhang, S. S. (2020). Problems and their origins of Ni-rich layered oxide cathode materials. *Energy Storage Mater.* 24, 247–254. doi:10.1016/j.ensm.2019.08.013